Theoretical Modeling and Electrochemical Behavior of Corrosion and Microbial Corrosion of Carbon Steel Pipelines

A. M. El-Shamy[(a)], F. A. Mohamed[(b)], W. M. Saad[(b)],, A. A. El-Bindary[(b)]*

Abstract—In this paper, inhibition of microbial and electrochemical corrosion by cinnamaldehyde at ambient temperature and pressure on carbon steel in aggressive saline conditions (3.5 % w/w NaCl solution) are pronounced. It is shown that, the cinnamaldehyde is a very virtuous microbial corrosion and corrosion inhibitor since the inhibiting effect being even higher at low concentrations. It was originating that, the cinnamaldehyde show highest efficiency in corrosion behavior but in situation of microbial corrosion, the results show moderate effect in planktonic and sessile bacteria. This correspondence notes the inhibitive properties of carbon steel corrosion reducing cinnamaldehyde in NaCl (3.5 % w/w) media. In NaCl medium the carbon steel coupons are presented with and without inhibitors. After the presentation, the samples were tested for open circuit potential, potentiodynamic polarization reactions, electrochemical impedance spectroscopy, and postmortem surface characterization of quantum chemical calculations. The optimum dosage and inhibition capacity of cinnamaldehyde is found to be 50 ppm, and 89.68%, respectively. The inhibition was believed mainly due to the adsorption mechanism on the metal surface of cinnamaldehyde. The findings obtained indicated that cinnamaldehyde's binding affinity to the metal surface was high relative to chemical adsorption since, it was associated with the modest increase in inhibition efficacy. The open circuit potential changed to a positive potential, and the calculations of polarization revealed that the antagonists were essentially mixed form of cathodic and anodic current densities diminished. The measured efficiency of inhibition, arising from potentiodynamic polarization and impedance spectroscopy, was found to be in good literature agreement. Observations from scanning electron microscopes demonstrated the presence of the inhibitor's protective adsorbed layer on the metal surface. Quantum chemical parameters have been determined and explained. The data demonstrated that cinnamaldehyde, thiourea, and sodium lauryl sulfate inhibition of carbon steel occurs by chemical adsorption process.

Index Terms— Corrosion inhibition; Cinnamaldehyde; Oil Field Industry; Microbial corrosion; Electrochemical techniques.

1 Introduction

The measured efficiencies in the inhibition using all corrosion control techniques were originated to be in respectable agreement with the previous studies [1-3]. DFT represents intense interactions between surface atoms Fe and S-atom where found to preferably occupy the resonating site among the hollow and bridge places on the Fe-surface, resulting in the formation of four strong Fe-S bonds that may explain the effective corrosion inhibition by thioureas on steels. The deterioration embarrassment of three α, β-unsaturated carbonyl mixtures on carbon steel were tested at higher temperature and in condensed acid media, and the mechanism of inhibition was studied. The consequence of cinnamaldehyde as an environmental barrier in reducing corrosion drawback to carbon steel in aerated NaCl (3.5 % w/w), the findings show modest cinnamaldehyde inhibition performance hitting about 70 % at an optimal level of 0.5 g/L or 500 ppm by forming an adsorption layer on the metallic superficial. The rate of corrosion reduced with dose of cinnamaldehyde to the optimal level, while at medium temperature gradually increased. The curves of polarization showed that the inhibitor performances as a mixed-type inhibitor since the current densities of anodic and cathodic branch are reduced. The inhibitive characteristics of AISI 1015 carbon steel deterioration extenuating cinnamadehyde in the NaCl (3.5% w/w) medium was inspected [4-6]. The statistics exposed that the binding attraction of cinnamadehyde on the metallic superficial was robust. In the attendance of sodium lauryl sulfate (SLS), Ni–Co_3O_4 amalgamated coverings were electrodeposited through a Watts-type bath to the surface of carbon steel [7-9]. The analysis showed that both cinnamaldehyde and benzal-acetone had a strong anticorrosive effect and could effectively mitigate steel decomposition in an acid medium The findings indicated that the transesterification reaction of α, β-unsaturated carbonyl composites on the steel superficial at high heat and in loaded acid materials occasioned in a positive cornea [10-12]. CoWxCy binder alloy's corrosion behaviors have been initiated to be the foremost component in WC–Co type hard metal chemical stability. CoW0·013C0·001 alloy anodic oxidation was tested as organic weathering inhibitors in 0·1 M H_2SO_4 with and deprived of additives of 20 mM sodium lauryl sulphate or 20 mM tri-sodium citrate. In this inquiry, linear sweep voltammetry, chronoamperometry, and ac impedance measurements (which may relay additional knowledge about processes of anodic activation that occur during corrosion) were used. Morphology and construction of the corrosion reaction is investigated through scanning electron microscopy and dispersive energy spectroscopy. This identified the inhibiting possessions of organic additives on the pseudo-passivating mechanisms [13-15]. This paper explores the sup-

- *(a) Physical Chemistry Department, Electrochemistry and Corrosion Lab., National Research Centre, El-Bohouth St. 33, Dokki, P.O. 12622, Giza, Egypt*
- *(b) Chemistry Department, Faculty of Science, University of Damietta, Damietta 34517, Egypt*
- *Corresponding author:* E-mail: *abindary@yahoo.com*

pression consequence of the various recorded Schiff centers on the degradation of HCl and H_2SO_4 media of carbon steel. Carbon steels have wide-ranging uses in the construction, industrial and petrochemical industries, where acid solutions like hydrochloric acid, sulfuric acid, are extensively applied as pickling or descaling agents. A suitable solution should be used as pickling solution to avoid the excessive oxidation of metal during pickling. Schiff bases are generally employed in these applications [16-18]. Compositions of decomposition suppressions that contain some variations of the subsequent components: a group 15 metal source, a compound of cinnamaldehyde, an additional compound of aldehyde, an acetylene compound, a surfactant, an iodide source, and a solvent. The compositions of the corrosion inhibitor can possess desirable environmental properties particularly for use in downhole environments [19-22]. A common procedure is the employ of additives to manage corrosion in metals and composites that are in interaction with hostile environment. Great sums of organic complexes have been recognized, and their capacity for corrosion inhibition is being explored. All these studies reveal that organic compounds showed considerable efficiency in inhibition, particularly those with N, S, and O. Yet, unfortunately, furthermost of these substances are not only harmful to human organisms but also poisonous. The value of inexpensive, effective corrosion inhibitors is unnecessary to argument out. Plant extracts have developed essential for a huge diversity of inhibitors as an ecologically friendly, readily accessible, and sustainable source which are considered as rich bases of constituents that are very effective in inhibitors [23-27].

2. MATERIALS AND METHODS

2.1 Chemicals and Solution

All required substances in this paper were acknowledged from saleable springs. The analytical-grade substances were applied deprived of additional decontamination. Ultra-pure NaCl, methanol, ethanol, cinnamaldehyde, thiourea and sodium lauryl sulfate were purchased from Sigma-Aldrich. Stock solution of corrosion inhibitors cinnamaldehyde, thiourea and sodium lauryl sulfate were organized with an organic solvent, methanol, and the final concentration of this organic solvent was less than 1%. The NaCl solution (3.5% w/w) was prepared by distilled water.

2.2. Preparation of Metal Coupon

The used coupons of carbon steel in this corrosion study were collected from local market. The carbon steel grade was predominantly explored through a distinctive conformation of (in wt. %). The average composition of the material used (in weight %) was: 0.097% C, 0.49% Mn, 0.020% P, 0.09% Si, 0.05% Cr, 0.11% Ni, 0.16% Cu, 0.042% S and Fe for the rest. Before exposure, the coupons were machined into 2×5×0.08 cm dimension and then mechanically abraded with 1200 grade of emery papers. The samples were subjected to grease removal with analytical-grade acetone and then left to dry at ambient temperature before experimental test.

2.3. Weight Loss Measurements

Weight loss assessments were done in a total capacity of 100 mL Pyrex vessel with, and without cinnamaldehyde, thiourea and sodium lauryl sulfate. To prepare diverse concentrations of cinnamaldehyde, thiourea and sodium lauryl sulfate an appropriate number of inhibitors were extracted from the stock solution and introduced directly to the corrosive test environment (3.5% w/w NaCl). The metal strips were engrossed in the solution and left for 1 week at 25 °C [28]. Following the 1-week exposure, the coupons were sensibly repossessed, cleaned in distilled water, and desiccated in open atmosphere before weighting. The preliminary wash removed incoherent fragments of film overlay covering the corroded samples. Several runs were performed for each set of conditions, and the mean value of the weight loss was recorded using a 4-digit analytical balance. The experiments were performed under aerobic conditions. The corrosion rate (CR) and inhibition efficiency (Ew %) were considered applying the subsequent equations (1-3):

$$CR\left(\frac{mg}{cm^2 h}\right) = \frac{\Delta m}{A.t} \quad (1)$$

Or

$$CR\left(\frac{mm}{year}\right) = 87.6\,\frac{\Delta m}{D.A.t} \quad (2)$$

$$E_w\% = \left[1 - \frac{W_{corr}}{W^o_{corr}}\right] X\,100 \quad (3)$$

where Δm (mg) is the change of the sample weight before and after engagement in the test solution, A is the area of the carbon steel coupon (cm2), t is the exposure time (h), and D is the metal density in g/cm3 (~7.8 g/cm^3). Wcorr and W◦corr are the weight losses for steel in the presence and absence of the inhibitor in NaCl solution, respectively [29-32].

2.4. Measurements of Potentiodynamic Polarization

Electrochemical measurements were carried out with the aid of an Auto lab potentiostat/galvanostat (PGSTAT302N), piloted by an Auto lab (NOVA) software, which facilitated ducting potentiodynamic sweeps in a conventional three-electrode setup hosted by a jacketed corrosion cell. A silver/silver chloride (Ag/AgCl) electrode and platinum electrode were used as reference and counter electrodes, respectively. The material used for constructing the working electrode was the same used for gravimetric measurements. The exposed area of the working electrode was machined in such a way that it assumed a square geometry with an exposed area of 0.5 cm^2. The experiments were performed at room temperature (25±1 °C). The working electrode was ground down to a surface finish of 4000 grit size using SiC abrasive paper. It was then polished as a mirror finish utilizing 1 (one) micron diamond paste. The finished surfaced was then rinsed thoroughly with deionized water before the commencement of electrochemical testing [33]. Polarization responses were sought without and with addition of various concentrations of cinnamaldehyde inhibitor (0.2, 0.5, 1, and 2 g/L) in 3.5% w/w NaCl solution at 25 °C,

while adopting a scan rate of 0.01 V/s. The test solution was de-aerated by purging with a moderate flow of nitrogen and agitation maintained by means of a magnetic stirrer for 10 min before starting the experiment. Potentiodynamic sweeps were obtained by commencing from cathodic realms of -0.8 to the more anodic 2.0 V Ag/AgCl. The purging process was maintained prior and throughout the experiments. The inhibition efficiency (IE%) was calculated using the following equation (4):

$$E_i\% = \left[\frac{j_{corr} - j'_{corr}}{j_{corr}}\right] X\ 100 \qquad (4)$$

where jcorr and j'corr are uninhibited and inhibited corrosion current densities, respectively.

2.5. Surface Analysis

APhilipsXL-30 field emission scanning electron microscope equipped with an Oxford instruments energy-dispersive X-ray detector was utilized both in secondary and backscattered electron modes with an accelerating voltage of 15 keV. The surface morphological characterizations and chemical analysis were pursued using the FESEM/EDX techniques. For surface analysis, the specimens were detached from corrosive medium, rinsed in distilled water to remove corrosion products, followed by washing with acetone and distilled water, and then dried in nitrogen flow.

2.6. Enumeration of Bacteria.

For the enumeration of bacteria, the most possible number (MPN) approach was used. The water sample was exposed to circulation in open air for 24 hours to enrich the planktonic bacterial growth, and then 1mL was used to estimate the bacterial counts. Synthetic Postgate media was delivered in test tubes, with 9 mL in each tube. The pumped water has been used to measure the biocidal capacity of the ionic liquids used by administering varying doses of the ionic liquids used.

3. Results and Discussion

3.1 Optimization. of Cinnamaldehyde Loading

Several loads of cinnamaldehyde were considered to theoretically reduce corrosion of carbon steel in a 3.5 % (w/w) NaCl solution to investigate optimal inhibitor dosing. Figure 1A and 1B demonstrates the evolution of deterioration rate and inhibition efficiencies (obtained from measurements of weight loss) in accordance with variability in inhibitor dose at ambient temperature and under aerobic conditions. By this statistic one can see that with raising the concentration of the inhibitor then the rate of corrosion fell dramatically and eventually settled down to a minimal value. With the initiation of 0.05 g/L (or 50 ppm) of cinnamaldehyde dosing, corrosion risk should be limited to a minimum corrosion rate. The same area of dosing of inhibitors correspondingly marked groundbreaking advances in receptor efficacy exceeding. Intrinsically, it may be deduced that optimum properties of cinnamaldehyde reduction can be considered residing close to 50 ppm. The deterministic explanation underlying such a phenomenon may be hypothesized as one concerning the spreading of cinnamaldehyde on the surface of carbon steel, which in effect contributes to the blockage of the reactive sites and prevents the metallic superficial beginning more setbacks expected from violent ions in the salt medium in the near-surface region [34]. It can therefore be inferred that cinnamaldehyde is an enough remedial step as far as corrosion of carbon steel is concerned in the 3.5 % (w/w) NaCl environment. The results fit well with previously mentioned researches [35-39].

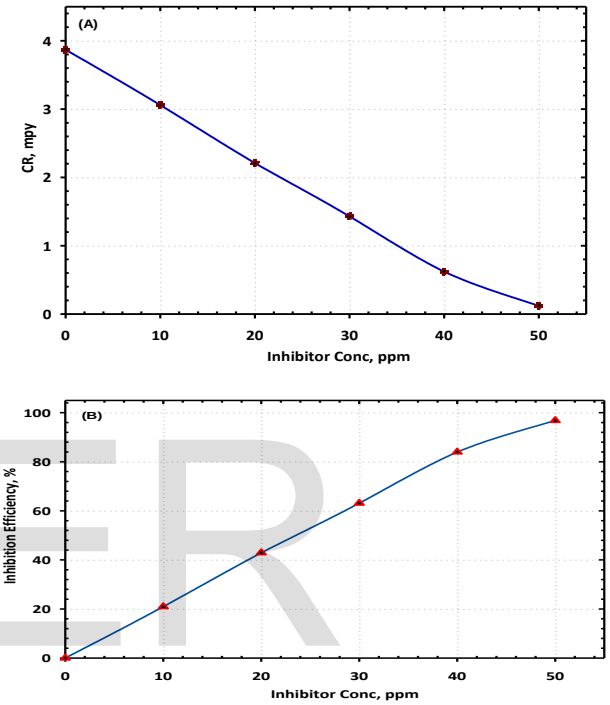

Figure 1. Effect of inhibitor concentration on (A) Corrosion Rate and (B) Inhibition Efficiency.

3.2. Corrosion Potentials

Figure 2 demonstrates the progression of Ecorr of the carbon steel electrode as a purpose of the disclosure time. The gained plot curves show that, the development of Ecorr at the initial podium alongside the extended coverage phase. The obtained plot curves suggest that, a comparable tendency as a function of concentration growth of corrosion inhibitor. Undeniably, for the duration of the initial time, Ecorr diminished in the first 50 seconds and reached the steady value and approximately stablished at 300 seconds. This phenomenon suggests that, the initiation of the deterioration progression, and illustrating the phenomenon of the de-passivation of the carbon steel electrodes [33]. Following that, the corrosion potential Ecorr growth considerably to more anodic magnitudes as a function of injection of serial concentration of the corrosion inhibitor. The intensification of corrosion potential has been recognized to the growth of pH of the electrolyte outstanding to the cathodic development which ascribed by the reduction of water and dissolution of oxygen that creates hydroxyl ions in the solution and the electrode surface became in the pas-

sivation state.

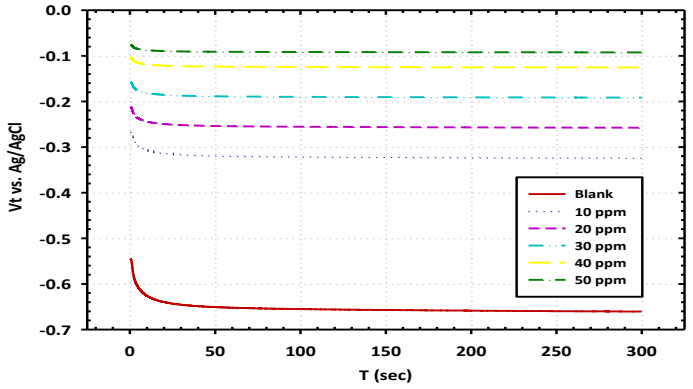

Figure 2. Corrosion potential evolution of carbon steel electrode without and with gradual concentration of cinnamaldehyde as a function of the exposure time in 3.5% NaCl solution at ambient temperature.

3.3. Measurements of Potentiodynamic Polarization

Typical carbon steel curves of Tafel polarization are obtained in 3.5 % (w/w) NaCl in the blank and injected of cinnamaldehyde inhibitors at several loads as publicized in Figure 3. Specific corrosion kinetics parameters such as corrosion potential (Ecorr), anodic and cathodic Tafel slopes (βa and βc), and corrosion current intensity (jcorr) were derived from the curve of Tafel polarization extrapolation (Table 1). The cathodic branch is the reaction of hydrogen evolution under the laboratory conditions conducted, while the anodic branch reflects the iron dissolution reaction. We are determined by Tafel lines being extrapolated to the consistent potentials of corrosion. As seen at Figure 3. The claim of cinnamaldehyde inhibitors has an inhibitive effect on both anodic and cathodic portions of the curves of polarization. It suggests a reversal of the cathodically hydrogen progression process, in addition to anodic steel dissolution. The findings indicate that cinnamaldehyde effectively inhibits the corrosion cycle of carbon steel, which is also noticeable created on the measured efficiency of inhibition, EI % (> 97 %) [40]. A strong curve was also found on both the anodic region and the cathodic region, in the injected sample with inhibitor. This bend is regarded as a plateau that shows passivation potential, i.e., oxidation-protection potential. Nevertheless, this spike was not originated in the control experiment pattern (3.5 % w/w NaCl alone) because it may deliberately corrode the metallic superficial. The findings showed that the significance of existing corrosion density (j_{corr}) was declined in the existence of an inhibitor. This activity reflects its ability in 3.5 % w/w NaCl solution to resist carbon steel corrosion. All the existing anodic and cathodic densities have been nearly diminished as seen in Figure 3, reporting that cinnamaldehyde mediated both anodic and cathodic reactions by adsorption on the surface of carbon steel. This indicates that against 3.5% NaCl solution, cinnamaldehyde functions as a mixed form corrosion inhibitor for carbon steel.

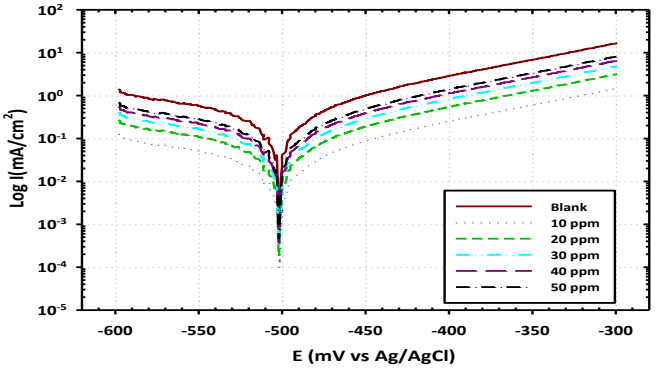

Figure 3. Potentiodynamic polarization curves of carbon steel electrode without and with gradual concentration of cinnamaldehyde in 3.5% NaCl solution at ambient temperature.

Table 1. The obtained corrosion parameters from the potentiodynamic polarization results for the carbon steel surface that was engrossed for dissimilar concentrations of cinnamaldehyde in 3.5% NaCl solutions.

Medium	Parameters						
	B_c mV dec^{-1}	E_{corr} V	j_{corr} μAcm^{-2}	B_a mV dec^{-1}	R_p Ωcm^2	R_{corr} mmy^{-1}	*I.E* %
Blank	-143.23	-0.6604	3512	85.11	6.85	59.09	---------
10 ppm	-142.95	-0.3251	3452	84.35	6.51	45.26	20.93
20 ppm	-138.24	-0.2562	3293	82.16	6.62	36.19	42.89
30 ppm	-130.65	-0.1916	3147	77.21	9.80	31.22	63.1
40 ppm	-126.41	-0.1230	2998	75.18	5.69	21.57	83.97
50 ppm	-123.35	-0.0938	2875	72.92	5.68	10.13	96.8

3.3.1. Electrochemical Impedance Spectroscopy (EIS) Measurements.

EIS measurements on the electrode of carbon steel were conducted to gain more knowledge about the inhibition mechanism. EIS can study relaxation phenomena in situ and non-destructive technique with a wide spectrum of frequency [41]. Figure 4A displays Nyquist and Bode carbon steel electrode plots in 3.5 % NaCl. Figure 4A displays the Nyquist plots obtained in 3.5 % NaCl as blank experiment for carbon steel and

existence of different TU and HMTA concentrations. Such conspiracies were categorized by a semicircular capacitive circle with high frequency. The Nyquist plot involves a loop of capacitance in a high frequency region, the middle of this loop lies underneath the actual axis, which is coupled to roughness, strong surface inhomogeneity or inhibitor adsorption. It is wrong observing that the higher frequency region will display primarily the inhibitor film's rapid responses [42,43]. The capacitance loop is associated to the load-transition resistance of the inhibitor film. Figure 4A designates that the capacitance loops become tighter as the concentration of inhibitors increases, mainly due to the accumulation of the receptor at the active sites on the carbon steel surface and the formation of a continuous film that exhibits a barrier. The remedy will help protection the metallic from hostile attack, which upsurges the confrontation to charge transfer. The log $|Z|$ − log f map is an oblique line in the medium frequency spectrum, suggesting that the device has a prevailing capacitive nature. At frequencies greater than 103 Hz, $|Z|$ values are roughly 1–3 cm^{-2} in solutions containing inhibitors except at the experiment containing 0.004M TU and 0.1M HMTA. Which indicates that in this area only the solution's resistance was observed. This can show certain rearrangements or a partial receptor desorption. The measures of in 0.004 M TU and 0.1 M HMTA slowly grow from 2 to 33 cm^{-2}, suggesting heavy correlations between metal surface and inhibitor and the process of desorption is difficult to occur. The equivalent circuit was used to match the EIS results, as seen in Figure 4B. Rs is the solution resistance in the corresponding circuit; Rct is the load transfer resistance; CPEdl1 and CPEdl2 denote the constant phase components describing the capacitance of the electric double layer and inhibitor film, respectively; and Rf denotes the resistance of inhibitor film [44]. The fitting parameters obtained using corresponding equivalent circuits are described in Table 2. According to Table 2, there are minor improvements to Rs. According to the capacitance concept, the variations in CPEdl can be due mainly to γ (the relative dielectric constant) and film thickness. The measure of ɪɪ in the pure NaCl solution is close to that of the constant of dielectric for gas. Since the inhibitor has been applied, the measure of ẏ is equal to the dielectric constant value for the inhibitors outstanding to the accumulation of the inhibitors on the superficial of the carbon steel; therefore, since adsorption, it will decrease. Around the same time the film's thickness would increase payable to the spreading of the inhibitors on the carbon steel surface. The sum of these influences leads to a Q2 fall. Since n is accompanying to superficial irregularity and heterogeneity, n=1 stands for an optimal capacitance, and n values check such findings as well. The n=1 slowly rises along with inhibitor concentration, which earnings that the film eventually became incorporated. The rise in Rct is indicative in slowly increasing the inhibitor film's charge transfer resistance, which is outstanding to the growth of shielding layer on the interface amongst metal and solution. Transformation of Kramers-Kronig (K-K) is also employed as an independent test on the validity of the impedance data. The transformation equations are most written as follows (Eqs. 5-7) when added to the EIS data [45]:

$$Z'(w) = Z'(\infty) + \frac{2}{\pi}\int_0^{\infty} \frac{xZ''(w) - wZ''(w)}{x^2 - w^2}\, dx, \quad (5)$$

$$Z'(w) = Z'(0) + \frac{2w}{\pi}\int_0^{\infty} \frac{(\frac{W}{x})Z''(w) - Z''(w)}{x^2 - w^2}\, dx, \quad (6)$$

$$Z''(w) = \frac{2w}{\pi}\int_0^{\infty} \frac{Z'(x) - Z'(w)}{x^2 - w^2}\, dx, \quad (7)$$

Where w is the frequency of translation, x is the frequency of integration, and Z′ and Z′′ denote the real and imaginary impedance components, respectively. Equations (1) and (2) provide the transformation of the imaginary axis-to-real axis, while (3) give the true transformation of the axis-to-imaginary axis. For five different etching solutions Figure 4C displays the impedance calculation and fitting defect. Of the various solutions, the chi-square errors for each impedance spectroscopy data set are $2.29x10^{-3}$, $3.97x10^{-3}$, $2.11x10^{-3}$, $6.37x10^{-3}$, and $1.72x10^{-3}$, respectively. As seen in Figure 4D, excluding at certain stages, the relative errors between the transition data and experimental data are in the region of 10 %. Because nearly of the system's spontaneous errors are expected, the investigational outcomes and the correct outcome should be in perfect accord. Consequently, the quintessential random spreading of the errors produced in the suitable data implies that the KK transitions are likeminded with the experimental results, and the corresponding circuit is an effective method for research.

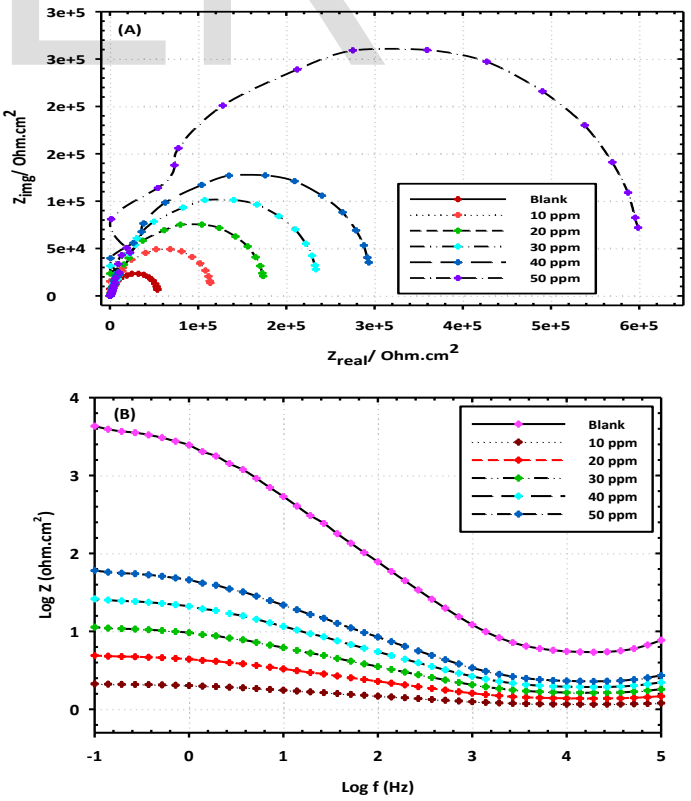

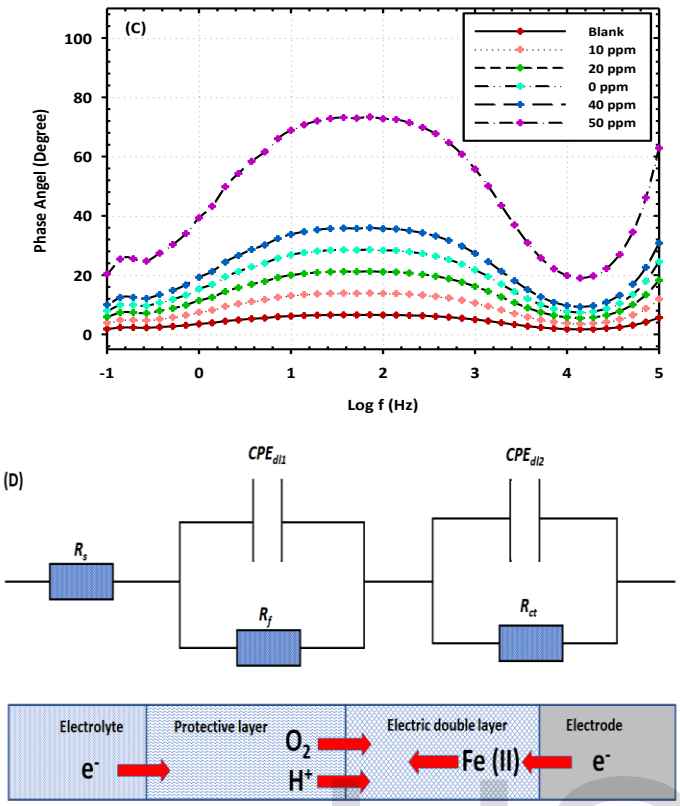

Figure 4. EIS Plots (A) Nyquist plot (B) Bode plots (c) Phase angle plots (D) Equivalent circuit.

Table 2. The obtained parameters by appropriate the EIS data through the corresponding circuit publicized in Figure 4 for carbon steel alloy steel in 3.5% NaCl solutions without and with serial concentration of cinnamaldehyde.

Medium	Parameters						
	R_s/ Ωcm^2	Yo/Fcm^2	n	R_{p1}/ Ωcm^2	R_{p2}/Ωcm^2	L/H	$I.E$, %
Blank	3.544	$1.9x10^{-4}$	128.21	12.676	4092	30.2	------
10 ppm	3.458	$2.1x10^{-4}$	1.440	17.552	9.826	30.616	21.92
20 ppm	4.412	$1.9x10^{-4}$	1.399	24.608	11.941	34.448	43.24
30 ppm	4.399	$1.9x10^{-4}$	1.749	35.361	14.297	37.428	64.33
40 ppm	6.109	$1.6x10^{-4}$	1.492	43.120	17.537	40.321	85.65
50 ppm	6.759	$1.3x10^{-4}$	1.285	49.639	18.214	38.214	97.81

3.4. Scanning Electron Microscopy (SEM)

The scanning electron micrographs were conducted to investigate the composition of the steel substrates with the inclusion of cinnamaldehyde and its absence. Figure 5A displays the untreated coupon SEM picture as leverage. Coupon surface is flat, so no pits of erosion are found. Figure 5B shows the morphology of coupons of 3.5 % (w/w) NaCl solution alone after being soaked for 7 days. The SEM picture showed that due to the violent attack of the 3.5 % (w/w) NaCl solution, the surface was very rough and badly affected. Large concentrations of corrosion materials are found on the soil. Figure 5C displays the SEM picture of the carbon steel surface exposed to 3.5 % (w/w) of NaCl for 7 days with the addition of 0.5 g/L (or 500 ppm) of cinnamaldehyde. From the figure the surface damage in the presence of cinnamaldehyde inhibitor has been greatly reduced. Compared to the surface treated with uninhibited 3.5 % (w/w) NaCl solution, a cleaner surface was found. It suggests that corrosion rate was abridged in the existence of the inhibitor, and a strong shielding coating was adsorbed on the metallic superficial that was responsible for corrosion inhibition.

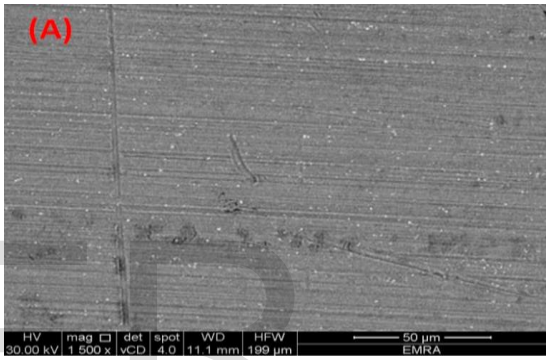

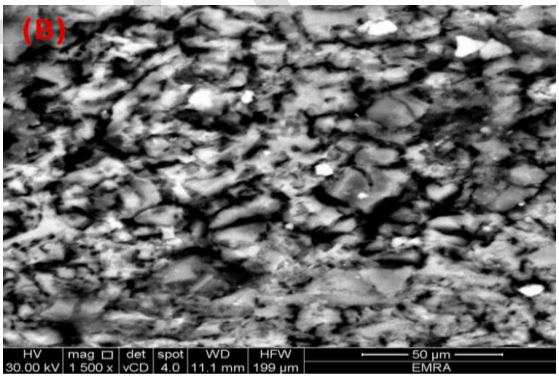

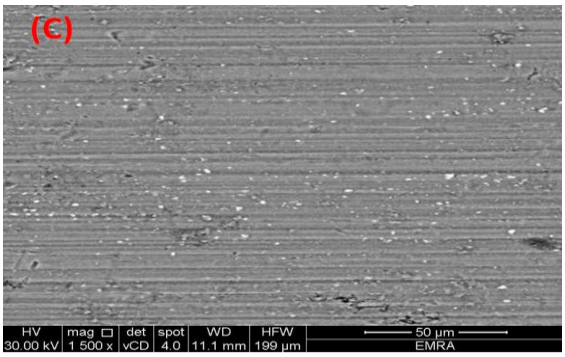

Figure 5. Scanning Electron Microscopy of (A) Polished sample (B) untreated sample (C) treated sample with 50 ppm cinnamaldehyde**.**

3.5. QUANTUM CHEMICAL CALCULATIONS.

The electronic requirements provide details about inhibitor-metal surface interaction. Quantum chemical equations seem to be the most widely employed way of understanding a molecule's electrical distribution. Many of the inhibitor properties determined from quantum chemical measurements are understood (Figure 6a). As shown in Figure 6a the optimized TU and HMTA geometries and Mulliken atomic charges. The negative atomic charges are typically the adsorbed core, so the electrons outside the negative atom can travel quickly to the unoccupied metal / metal oxide orbital. The electronic specifications provide details about inhibitor-metal surface interactions. Quantum chemical equations are the greatest and extensively applied way of understanding a molecule's electrical distribution. Several properties of the inhibitor can be determined from quantum chemical measurements are seen in Figure 6b [46–49]. Figure 6b displays the optimized TU and HMTA geometries and Mulliken atomic charges. The negative atomic charges are typically the adsorbed core, so the outside electrons the negative atom can travel quickly to the vacant orbital metal / metal oxide orbital. Figure 6c displays that for any regulator the most negative atomic charges exist in the N atomics. For TU and HMTA, the N atomic charges are −0.829 and −0.305, respectively. This means N is readily combined into the of carbon steel surface as it relative to other atoms. Furthermore, the description of the highest occupied molecular orbital (HOMO) and the lowest unoccupied molecular orbital (LUMO) confirms that the heterocyclic ring is strongly inclined to pass electrons to metal surfaces. As seen in Table 3, the quantitative values of the quantum chemical parameters are determined. Due to Fukui's frontier molecular orbital theory of chemical reactivity, much of the electron transfer will occur at the frontier orbitals, called the reacting species HOMO and LUMO. HOMO's energy (EH) is closely interrelated to the propensity for ionization and symbolizes the molecule's susceptibility to electrophile attacks; it is an indicator of inhibitor power for electron endowment and describes the adsorption on surfaces of carbon steel by means of delocalized free electrons. The EH for HMTA is −477.6 and −483.6 kJ.mol^{-1} for each. This means the HMTA bond designed on the surface of carbon steel is tougher than TU's. The LUMO energy (EL), which stances for the capacity of obtaining electron inclination, is specifically associated with the affinity of the electron and symbolizes the molecule's susceptibility to nucleophilic assault [50,51]. The smaller the EL levels, the greater the willingness of the particles to accept the electron. Carbon steel LUMO can accept inhibitor electron in HOMO. Depending on these criteria, the measured difference (alternatively = E_{LUMO} – E_{HOMO}) indicates the intrinsic donation potential of electron and tests the inhibitor molecule's contact with surface of carbon steel. The measurements of ΔE for TU and HMTA are 432.5 and 575.9 kJmol^{-1}. Since the small-E molecules have stronger reactivity than the large-E molecules, it may be inferred that TU has more resistance to the carbon steel surface. The consequence of inhibitor dipole moment, μ, produces a large static electrical field that contributes to surface energy bending upwards / downwards. TU's dipole moment is 3,545 Debye's, from Table 3. Therefore, polar molecules still exist. The interpretation of the TU in solution such as water and H+ molecule can interact with other polar molecules. The simulation tests are confirmed by experimental findings [52]. For TU, the solution has excellent contact with liquids. The TU film would also have an ocean of deficits. Some other parameters are also determined, such as ɪɪ, ɪɪ, and ombN. According to the Hartree-Fock theorem; the ionization potential (I) and the electron affinity (A) are given by equations 8 and 9:

$$I = -E_{HOMO} \quad (8)$$

$$A = -E_{LUMO} \quad (9)$$

Their practical and provisional definitions for absolute electronegativity, ÿ, and global hardness are as follows (Eqs. 10 and 11):

$$\chi = \frac{I + A}{2} \quad (10)$$

$$\eta = \frac{I - A}{2} \quad (11)$$

Two processes are put together, carbon steel and inhibitor, and electrons will flow from lower x (inhibitor) to higher x (carbon steel), till the chemical potentials are equivalent. The segment of the transfer of electrons ΔN, is given as follows (Eq. 12) [53,54]:

$$\Delta N = \frac{(X_{carbon\ steel} - X_{inhibitor})}{2(\eta_{carbon\ steel} + \eta_{inhibitor})} \quad (12)$$

To quantity the portion of electrons transported, a numerical value for the absolute electronegativity of carbon steel based on Pearson was applied for carbon steel = 463.1 kJmol^{-1} and a global hardness of carbon steel = 0, suggesting that the Fe atoms are weaker than the neutral metallic atoms. Global hardness, ÿ, is a parameter that provides crucial knowledge about the molecule's reactive nature. The values for TU and HMTA are respectively 216.3 and 287.9
kJmol^{-1}. The determined order of reactivity for the derivatives in the aqueous phase inhibitors is thus TU > HMTA. ÊN is the numeral of electrons passed from the barrier to the carbon fiber surface Figure 6d. The values of the inhibition reaction produced by ΔN derived from donation of electrons. If

ΔN<3.6, the efficiency of inhibition will be increased by snowballing the donation potential of electron on the metallic superficial. It can be inferred from Table 3 that TU and HMTA have greater capacity of electrons to contribute to shape inhibitive adsorption layers [55].

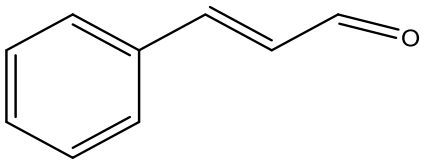

Figure 6a. Chemical formula of cinnamaldehyde

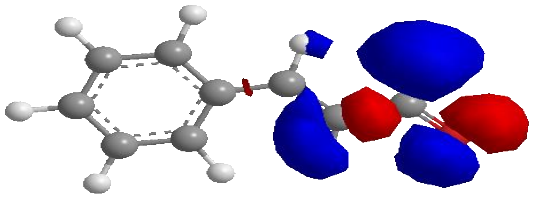

Figure 6b. HOMO skeleton of cinnamaldehyde.

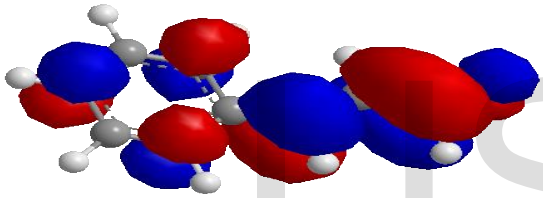

Figure 6c. LUMO skeleton of cinnamaldehyde.

Table 3. Energy values obtained in docking calculations of cinnamaldehyde.

Est. Free Energy of Binding	Est. Inhibition Constant, Ki	vdW + Hbond + desolv Energy	Electrostatic Energy	Total Intermolec. Energy	Frequency	Interact. Surface
-4.54 kcal/mol	468.07 uM	-5.09 kcal/mol	-0.04 kcal/mol	-5.13 kcal/mol	100%	416.407

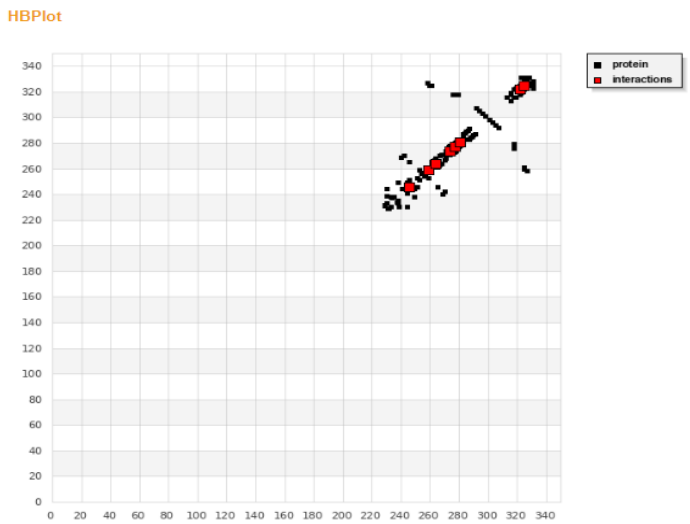

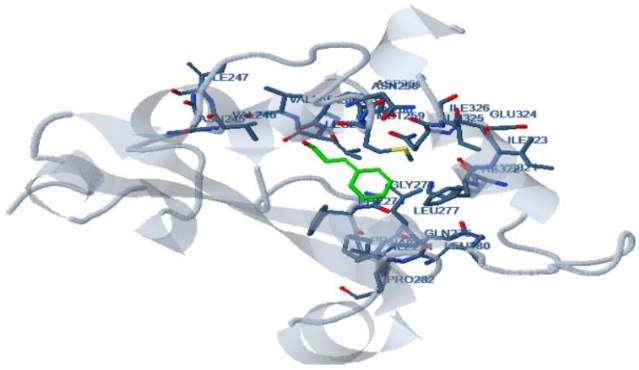

Figure 6d. Protein interaction pattern of cinnamaldehyde

3.6. Inhibition Mechanism.

Two forms of mechanism for inhibition have usually been suggested. This was the formation of polymeric complexes with ions from carbon steel according to the conditions applied. Others formed a defensive layer on the carbon steel surface [56]. According to the study, this inhibitor's inhibition function can be calculated as being the second. The complex phase of protecting layer forming can be demarcated as below. Once the inhibitors are injected to the solution, foremost to the spreading of the receptor fragments on the surface, the reactive metal structure transitions into the inactive state. The spreading of the inhibitor can be represented mainly by chemisorption, which will occur by TU and HMTA's N and S outstanding to its intrinsic capacity to contribute electrons. TU has the intrinsic potential of electron donors to the metallic superficial owing to the lower values of ΔE and π; it also interacts actively with the solution's water molecules. Since it is a polar fragment of μ = 3,545, just 69,911 $kJ.mol^{-1}$ is the strength of contact between metal surface and TU. With HMTA the situation is the reverse. While HMTA has a greater intrinsic potential to transfer electrons to the metallic superficial than TU, it has disgusting belongings on water molecules as it is a nonpolar fragment with μ = 0.014. Combining the two not only improves the quality of the films but also strengthens the protection to the penetration of oxygen fragments from the solvent to the carbon steel surface.

3.7. Antibacterial Effect of Cinnamaldehyde

Figure 7A and B indicates the bacterial development because of time in the absence of used cinnamaldehyde. It is easily shown that; the bacterial counts rise after 24 hours with time hitting a value of 106. Instead different doses of cinnamaldehyde were administered to study the effect of the cinnamaldehyde used on the growth inhibition of the planktonic bacteria. It investigated the influence of cinnamaldehyde on planktonic bacteria growth. Figure 7 shows the decay of the bacterial

counts by increasing the time at different cinnamaldehyde concentrations. As seen in Figure 7A, the bacterial counts are reduced linearly by time at a concentration of 100 ppm, and a total inhibition of bacterial growth is achieved after 6 hours of injection. By increasing the concentration of cinnamaldehyde, the degree of inhibition of bacterial growth increases, and at a concentration of 100 ppm the maximum result was observed. At a concentration of 100 ppm of 100 colony/mL was calculated after 1 hour of injection, and a full inhibition was achieved after 3 hours. The improvement in the bacterial growth inhibition efficiency in the presence of different cinnamaldehyde concentrations is shown in Figure 7B. The efficacy of the injected cinnamaldehyde in inhibition was calculated using the following equation 13:

$$IE\ (\%) = \frac{Bacterial_c - Bacterial_{c(inh)}}{Bacterial_c} X\ 100 \qquad (13)$$

where $Bacterial_c$ and $Bacterial_{c(inh)}$ are the bacterial counts in absence and in the presence of the cinnamaldehyde, respectively.

As seen in Figure 7B, the bacterial growth inhibition efficiency improved as the cinnamaldehyde concentration rose. At a concentration of 25 ppm of cinnamaldehyde the bacterial growth inhibition output exceeded 90 percent in one hour, and about 99.9 percent was achieved after three hours. Nevertheless, an inhibition output of around 99.99 per cent was obtained in one hour at a concentration of 100 ppm. Such findings suggest the bactericidal activity of cinnamaldehyde, and the efficacy of inhibition was based on concentration of cinnamaldehyde. In general, the cinnamaldehyde's antibacterial effect is due to the cell membrane's attraction of the cinnamaldehyde species which causes its disruption [57]. The cinnamaldehyde's influence on planktonic growth of bacteria. As for cinnamaldehyde, the presence of cinnamaldehyde resulted in a substantial reduction in the bacterial counts, for concentration-dependent levels. Given the above findings, it could be inferred that the ionic liquids used could in theory be used effectively as efficient biocides to reduce bacterial growth, which in turn contributed to regulation of microbially induced corrosion. As is known, the colonization of bacteria on a metal surface will facilitate biofilm formation. This can cause local gradients of dissolved oxygen, pH, and corrosive anions which, in effect, result in acceleration of corrosion [58]. Thus, reducing the microbially mediated corrosion requires inhibition of bacterial growth rate.

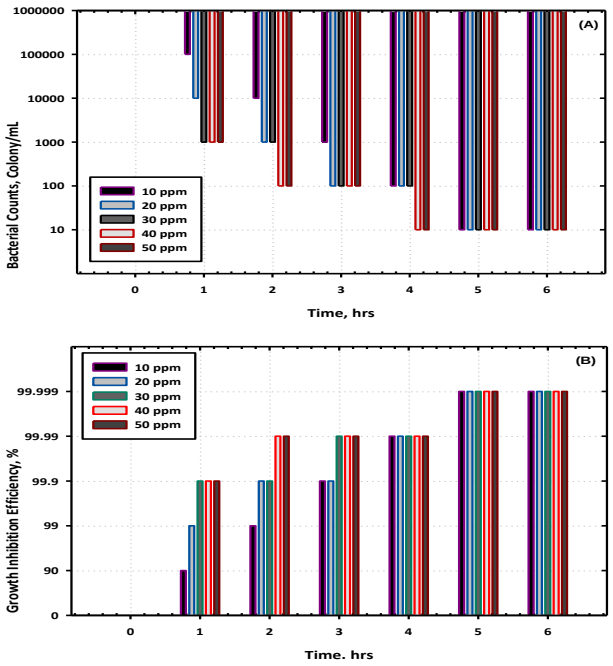

Figure 7. Effect of cinnamaldehyde concentration on the (A) biocidal activity and (B) growth inhibition efficiency at different time.

4. Conclusions

Cinnamaldehyde as an environmentally safe corrosion inhibitor has been explored in this paper. Cinnamaldehyde was initiated to work against the corrosive atmosphere as an important corrosion inhibitor for carbon steel, in 3.5 % w/w NaCl solution. With the initiation of 200 ppm cinnamaldehyde dosing, the average inhibition efficiency was originated to be 95.36 %. Cinnamaldehyde's binding affinity to the surface of carbon steel was high, with a widespread temperature range. Cinnamaldehyde adsorption on surfaces of carbon steel obeys the isotherm Langmuir. Parameters of thermodynamic adsorption suggested that the mode of action of dissolution of carbon steel is of an endothermic nature and indicates that adsorption of cinnamaldehyde may occur by both physisorption and chemical adsorption. Curves of potentiodynamic polarization have been proved that, the cinnamaldehyde inhibits mutually anodic and cathodic reactions, suggesting that it is an inhibitor of a mixed sort. The efficiencies of metabolites measured by methods of electrochemical polarization and gravimetric analysis (weight loss) and it is found that, there is a good agreement with the world trends. SEM measurements showed that, the corrosion of carbon steel in 3.5 % w/w NaCl was mitigated during treatment by introducing cinnamaldehyde inhibitors into the violent media. Hence, cinnamaldehyde may be considered a remedial step and plausibly employed as a possible eco barrier for other metals and composites in the future. The Langmuir isotherm will explain the

adsorption of the mixture on the carbon steel surface, the maximum surface coverage is 0.981, and the free adsorption energy is −35.50 kJmol^{-1}. The inhibitor inhibition process involves the progress of a protecting layer on the carbon steel surface, due primarily to chemisorption. The defensive layer can sever corrosive particle diffusion coefficients.

REFERENCES

[1] S. M. Z. Hossain, S. A. Kareem, A. F. Alshater, H. Alzubair, S. A. Razzak, M. M. Hossain, *Arab. J. Sci Eng.*, 45 (2020) 229–239.

[2] A. M. El-Shamy., T. Y. Soror., H. A. El-Dahan., E. A. Ghazy., A. F. Eweas, *Mater. Chem. Phys*., 114 (2009) 156-159.

[3] S. M. Z. Hossain., A. Al-Shater., S.A Kareem., A. Salman A., R. A Ali., H. Ezuber., M. M. Hossain., S. A Razzak., *Arab. J. Sci. Eng.*, **44**(2019) 5489–5499.

[4] A. M. El-Shamy., K. M. Zohdy., H. A. El-Dahan, *Ind. Chem.)* 2016, 2:2 DOI: 10.4172/2469-9764.1000120.

[5] K. O. Nayana, S. Ranganatha., H. N. Shubham., *Metals Soc. China*, 29 (2019) 2371-2383.

[6] A. M El-Shamy., K. M. Zakaria. A. Abbas, S. Z. El Abedin, *J. Mol. Liq*., 211 (2015) 363-369.

[7] Gao Jiancun, Weng Yongji1, Pet. Sci. 6(2009).201-207.

[8] F. M. Alkhrafi, A. M El-Shamy, B. G. Ateya, *Int. J. Electrochem. Sci*., 4 (2009) 1351–1364.

[9] B. Bozzini, G. P. De Gaudenzi, C. Mele, Pages 290-300 (2013). 27 Nov 2013 Published online.

[10] A. M. El-Shamy, M. F. Shehata, S. T. Gaballah, E. A. Elhefny, *J. Adv. Chem*., 11(2) (2015) 3441-3451.

[11] A. I. M. Ismail, A. M.,El-Shamy, *Appl. Clay Sci*., 42 (2009) 356-362.

[12] P. Shetty, *J. Chem. Eng. Comm.*, 207 (2020).

[13] B. G. Ateya, F. M. Alkharafi, A. M. El-Shamy, A. Y. Saad, *J. Appl. Electrochem*., 39 (2009) 383–389.

[14] A. M. El-Shamy , M. A. A. Elkarim., A. Kalmouch, *J. Chem. Eng. Process. Technol*., (2017)1-7.

[15] M. M..Solomon, S..A Umoren, I. B. Obot, A. H. Sorour,H. Gerengi, ***A****CS Appl. Mater. Interf*., 10 (2018) 28112–28129.

[16] A. M. El-Shamy, K. M. Zohdy, *J. Appl. Chem. Sci. Int*., 2 (2015) 56-64.

[17] F. Mohamed, F. Shehata, A. M. El-Shamy, K. M. Zohdy, M. El-Sayed, S. Z. El-Abedin, *Appl. Sci*., 10(4) (2020) 1444.

[18] A. M. El-Shamy, H. K. Farag., W. M. Saad, *Egypt. J. Chem*., 60 (2017) 1165-1175.

[19] F. M. Alkharafi, A. M. El-Shamy, B. G. Ateya, *J. Chem. Eng*., 3 (2009) 42-50.

[20] A. M. El-Shamy, S. T. Gaballah, A. E. El-Meleigy, *Int. J. Rec. Develop. Eng. Technol*., 1 (2) (2013).11-18.

[21] M. Shehata, S. El-Shafey, N.A. Ammar, A. M. El-Shamy, *Egyp. J. Chem*., 62 (2019) 1587-1602.

[22] Y. Reda, A. M. El-Shamy, K. M. Zohdy, A. K Eessaa, *Ain Shams Eng. J*., 11 (2020) 191–199.

[23] Y. Reda, K. M. Zohdy, A. K. Eessaa, A. M. El-Shamy, *Egypt. J. Chem*., 63 (2020) 579–597.

[24] Y. Reda, A. M. El-Shamy, A. K. Eessaa, *Ain Shams Eng. J*., 9 (2018) 2973–2982.

[25] H. Jafferji, A. R. Sakulich, J. D.Schiffman. Concrete Compos.69 (2016) 9–17.

[26] A. M. El-Shamy, I. Abdelfattah, O. I. Elshafey, M. F. Shehata, *J. Environ. Manag*., 219 (2018) 325-331.

[27] F. Zucchi, G. Trabanelli, G. Brunoro, Corros.Sci. 36 (1994) 1683–1690.

[28] A. M. El-Shamy., M. F. Shehata., H. I. M. Metwally, A. Melegy, *Silicon*, 10 (2018) 2809-2815.

[29] L. Messaadia, O. Id El Mouden, A. Anejjar, M. Messali, R. Salghi, O. Benali, O. Cherkaoui, A. Lallam, *J. Mater. Environ. Sci*., 6 (2015) 598–606.

[30] R. Javaherdashti, C. Nwaoha, H. Tan, A. M. El-Shamy, Taylor & Francis Group. Chapter Cathodic Protection in the Oil and Gas Industry, p, (2013) 489-510.

[31] Neelam Garg and Abhinav Aeron. Microbes in Process. NOVA Science Publishers. Chapter 14, Control of Corrosion Caused by Sulfate-Reducing Bacteria, p, 337-362 (2014).

[32] S. Ranganatha, T. V. Venkatesha, K. Vathsala, M. K. P. Kumar, *Surf. Coat. Tech*., 208 (2012) 64–72.

[33] A. M. El-Shamy, M. A. El-Hadek, A. E. Nassef, R. A. El-Bindary, *J. Chem*., 2020 (2020) Article ID 9212491.

[34] X. Li, J. Wang, E. H. Han, W. Ke, Corros. *Sci*., 67 (2013) 169–178.

[35] K. M. Zohdy, A. M. El-Shamy, A. Kalmouch, E. A. M. Gad, *Egypt. J. Petroleum*., 28(4) (2019) 355–359.

[36] J. Hu, Q. Duan, G. Cheng, Z. Zhang, X. Chen, B. Wang, ,58 (2013) 25–32.

[37] A. M. El-Shamy, H. A. El-Boraey, H. F. El-Awdan, *J. Chem. Eng. Process. Technol*. 2017 (2017) 1-8.

[38] T. Tuken, B. Yazici, M. Erbil, *Surf. Coat. Tech*nol., 200 (2006) 4802–4809.

[39] A. M. El-Shamy, F. M. Shehata, A. I. M. Ismail, *Appl. Clay Sci.*, 114 (2015) 461-466.

[40] S. Skale, V. Dolecek, M. Slemnik, *Sci*., 49 (2007) 1045–1055.

[41] A. M. El-Shamy, F. M. Alkharafi, R. M. Abdallah, I. M. Ghayad, *Chem. Sci. J*., 2010 (2010) 1-12.

[42] M. Behpour, N. Mohammadi, *Sci*., 65 (2012) 331–339.

[43] F. Bentiss, M. Lagrenee, B. Elmehdi, B. Mernari, M. Traisnel, H. Vezin, *Corros*., 58 (2002) 399–407.

[44] E. M. Sherif, A. T. Abbas, H. Halfa, A. M. El-Shamy, *Int. J. Electrochem. Sci*., 10 (2015) 1777–1791.

[45] I. Lukovits, E. Kalman, F. Zucchi, Corros., 57 (2001) 3–8.

[46] K. F. Khaled, Corros. Sci., 52 (2010) 3225–3234.

[47] E. M. Sherif, A. T. Abbas, D. Gopi, A. M. El-Shamy, J. Chem., (2014) Article ID 538794.

[48] S. Zor, M. Saracoglu, F. Kandemirli, T. Arslan, 67 (2011) Article ID 125003.

[49] L. A. F. Costa, H. S. Breyer, J. C. Rubim, Vibrat. Spectro., 54 (2010) 103–106.

[50] A. A. Mohamed, K. Zakaria, A. M. El-Shamy, S. Z. El Abedin, Zeitschrift für Physikalische Chemie (2020).

[51] D. Gelman, D. Starosvetsky, Y. Ein-Eli, Corros. Sci., 82 (2014) 271–279.

[52] A. Doner, R. Solmaz, M. Ozcan, G. Kardas, Corr. Sci., 53 (2011) 2902–2913.

[53] V. S. Sastri, J. R. Perumareddi, Sci. Res., 53 (1997) 617–622.

[54] H. Ju, Z. P. Kai, Y. Li, Sci., 50 (2008) 865–871.

[55] K. F. Khaled, S. A. Fadl-Allah, B. Hammouti, Mater. Chem. Phys., 117 (2009) 148–155.

[56] A. M. El-Shamy, M. A. El-Hadek, A. E. Nassef, R. A. El-Bindary, Mor. J. Chem., 8 (2020) 788-800.

[57] N. B. Ibsen, H. Ma, A. Banerjee, E. E. Tanner, S. Nangia, S. Mitragotri, Sci. Eng., 4 (2018) 2370–2379.

[58] Z. Lewandowski, H. Beyenal, Mechanisms of microbially influenced corrosion. In Marine and Industrial Biofouling, Springer, Berlin, Germany, pp. 35–64 (2009).